Supplementary Materials for

21st century rise in anthropogenic nitrogen deposition on a remote coral reef

Haojia Ren,* Yi-Chi Chen, Xingchen T. Wang, George T. F. Wong, Anne L. Cohen, Thomas M. DeCarlo, Mira A. Weigand, Horng-Sheng Mii, Daniel M. Sigman

*Corresponding author. Email: abbyren@ntu.edu.tw

Published 19 May 2017, *Science* **356**, 749 (2017)
DOI: 10.1126/science.aal3869

This PDF file includes

Materials and Methods

Coral core collection and age model

The two coral skeletal cores were collected from living *Porites* sp. colonies in June 2013 using an underwater pneumatic drill. The north reef flat core ("751") was drilled to the base of the colony and reached 1 m in length, whereas the east lagoon core ("762") is 0.5 m in length. Both corals lived in approximately 2 m deep water. The cores were passed through the Siemens Volume Zoom Spiral computed tomography (CT) scanner at Woods Hole Oceanographic Institution. Skeletal density was determined from the CT scans following the methods of (*34*). Annual calcification rates (g cm^{-2} yr^{-1}) were calculated as the product of annual density (g cm^{-3}) and extension (cm yr^{-1}), measured using the automated software program coralCT (*35*).

The age model determined by counting annual growth bands in CT scan images was validated by comparing skeletal $\delta^{18}O$ with satellite sea-surface temperature by matching midpoints of $\delta^{18}O$ and SST (Figure S3). We observe a good correlation when comparing this remote sensing SST product with higher resolution NOAA SST product and with *in situ* measurement of SST from the northern reef flat.

Methods for CS-$\delta^{15}N$ analysis

The protocol follows and is modified from that of (*14*). First, in an oxidative cleaning step to remove external/contaminant organic matter, 10 mL sodium hypochlorite (10–15% available chlorine) is added to ~20 mg of coral powder in 15 mL centrifuge tubes and agitated for 12 hours. The cleaning reagent is decanted, and the sample is rinsed 3 times with deionized water by centrifugation and decanting and then dried at 60 °C. Once dry, cleaned coral (~10 mg per sample) is weighed into a 4 mL borosilicate glass vial (precombusted for 5 hrs at 500 °C) and dissolved in 4N HCl. Purified basic potassium persulfate oxidizing solution is added to each vial, and the vials are then autoclaved for 1 h on a slow-vent setting to completely oxidize to nitrate the organic nitrogen released during decalcification. To lower the N blank associated with the oxidizing solution, the potassium persulfate is recrystallized three times. At the time of processing, 0.8 g NaOH and 0.5 g potassium persulfate are dissolved in 100 ml of deionized water. Organic standards are used to constrain the $\delta^{15}N$ of the persulfate reagent blank. We use three organic standards: USGS 40 ($\delta^{15}N$ = -4.5‰ *vs*. air), USGS 41 ($\delta^{15}N$ = 47.6‰ *vs*. air), and a self-made mixture of 6-aminocaproic acid and glycine ($\delta^{15}N$ = 5.4‰ *vs*. air). A minimum of 18 organic standards and 3–5 blanks are analyzed per batch of samples.

After oxidation, the sample is centrifuged, the clear supernatant is transferred to another precombusted 4 mL borosilicate glass vial, and the pH of the supernatant is adjusted to near 7 with HCl and NaOH. To determine the N content of the samples, we measure nitrate concentration in the oxidation solutions after autoclaving. Nitrate concentration is analyzed by reduction to nitric oxide using vanadium (III) followed by chemiluminescence detection (*36*). The N blank is also quantified in this way. Consistent with previous findings, *Porites* corals have an average N content of 3 μmol N per gram of clean aragonite, yielding nitrate concentrations in the oxidation solutions of ~30 μM, whereas the blank concentration ranges between 0.3 and 0.7 μM (less than 3%, typically

less than 1%, of the total N per sample).

The $\delta^{15}N$ of the samples is determined using the denitrifier method in conjunction with gas chromatography and isotope ratio mass spectrometry (*37, 38, 46*). The denitrifier method involves the transformation of dissolved nitrate and nitrite into nitrous oxide gas (N_2O) via a naturally occurring denitrifying bacterial strain that lacks an active form of the enzyme N_2O reductase. The denitrifier *Pseudomonas chlororaphis* was used for this work. Normally, 5 nmol sample amounts are added to 1.5 ml of bacterial concentrate after degassing of the bacteria. Along with the samples, the organic standards as well as replicate analyses of nitrate reference material IAEA-NO3 ($\delta^{15}N$ = 4.7‰ *vs*. air) and a bacterial blank are also measured. We use the IAEA-NO3 standards to monitor the bacterial conversion and the stability of the mass spectrometrer, and we use the oxidation standards to correct for the oxidation blank. If possible, samples are oxidized in duplicate, and oxidized samples are analyzed by the denitrifier method in duplicate when possible. The denitrifier method typically has a standard deviation (1sd) of less than 0.1‰. An in-house coral standard (CBS-1) provides a metric for repeatability both within an analysis batch and across batches, which indicates an analytical precision (1sd) of our protocol of 0.2‰.

The *Porites* cores at the north reef flat and east end of lagoon show similar CS-$\delta^{15}N$ values and the same seasonal variation (Figure S1). This demonstrates the robustness of our analytical method and also speaks to the reliability of CS-$\delta^{15}N$ for recording reef-wide $\delta^{15}N$ dynamics.

Methods for nitrate sampling and $\delta^{15}N$ analyses around Dongsha

Discrete water samples were collected within and surrounding Dongsha Atoll (Figure 1B white triangles) in the summers of 2012 and 2013 aboard the R/V *Ocean Researcher III*, with GO-FLO bottles mounted onto a Rosette sampling assembly. From each depth, unfiltered seawater was collected in a rinsed 60 ml HDPE bottle and immediately frozen at -20°C.

The $\delta^{15}N$ of nitrate was also determined using the denitrifier method, as described above (*37, 38, 46*). We use two international nitrate isotope reference materials, IAEA-NO3 ($\delta^{15}N$ = 4.7‰ *vs. air*) and USGS-34 ($\delta^{15}N$ = -1.8‰ *vs. air*), to normalize the seawater nitrate $\delta^{15}N$ data to atmospheric N_2 ("air"). Averaging across the broad range of nitrate concentrations encountered, long term analytical precision (1sd) for $\delta^{15}N$ was 0.08‰.

Nitrate $\delta^{15}N$ in the waters surrounding Dongsha is similar to observations from South East Asia Time Series Station (SEATS) (Figure S2). The shallow subsurface nitrate $\delta^{15}N$ (~80m) around Dongsha is 5.5±0.2‰. It is lower than deep (i.e. ≥300 m) nitrate $\delta^{15}N$ in the northern South China Sea, a regional feature originating from input of ^{15}N-depleted source through N fixation (*9*), and it characterizes the $\delta^{15}N$ of the primary oceanic N source to the surface of Dongsha, as the nitrate supplied from below is essentially completely consumed in the euphotic zone. Despite the low nitrate concentration, we were able to analyze the $\delta^{15}N$ of surface nitrate just below the base of mixed layer (30-50 m). It is higher than the $\delta^{15}N$ of subsurface nitrate, as a result of partial nitrate assimilation between the mixed layer and the base of the euphotic zone. Similarly, elevated surface nitrate $\delta^{15}N$ is found both at SEATS and in the Sargasso Sea

during warm stratified seasons when the base of the euphotic zone is below the mixed layer (*39*).

Supplementary Text

Calculation of the fraction of atmospheric N deposition in the total N input to the surface of the northern South China Sea

The $\delta^{15}N$ of the total N supply to the euphotic zone of the northern South China Sea should equal the weighted sum of vertical N supply, N fixation, and atmospheric N deposition. Based on existing data, we assume that the $\delta^{15}N$ for oceanic nitrate, N fixation, and atmospheric N deposition are 5.5‰, -1‰ (*10*) and -2.7‰ (*11*) respectively, which are the end members in the surface ocean N budget and isotope balance model.

The $\delta^{15}N$ of oceanic nitrate to Dongsha Atoll is 5.5‰, similar to the upper thermocline nitrate $\delta^{15}N$ in the northern South China Sea measured in 1997 and from 2012 to 2013 (~5‰) (*9*) (Figure S2). In addition, there is no long-term change in the N* in the upper water column from 1999 to 2004 (*19*). These argue for a stable oceanic N source with a constant $\delta^{15}N$; this is expected given the short time period over which AAN deposition has risen, combined with the tendency of circulation to homogenize subsurface nitrate and its $\delta^{15}N$ across the basin and between the basin and the open western North Pacific. The $\delta^{15}N$ of water-soluble nitrate in bulk atmospheric deposition at Dongsha Atoll is measured to be -2.7‰ averaged for dry and wet deposition from 2010 to 2011 (*18*). We take this value to represent the $\delta^{15}N$ value for AAN deposition at our site. While more work is needed to characterize the different components in the atmospheric N deposition and their origins and isotopic signatures, our assumed $\delta^{15}N$ (-2.7‰) falls within the reported range for atmospheric N deposition in oceanic regions and is on the higher $\delta^{15}N$ end reported for anthropogenic N deposition to the ocean (*40-42*). In this regard, our calculations would tend to overestimate the increase in AAN deposition, further supporting the assertion that AAN deposition has increased less than previously suggested (see main text).

We construct our model with the following equations:

$$F_{N\ fixation} + F_{atm\ N} + F_{oceanic\ N} = TotN \quad (1)$$

$$\delta^{15}N_{N\ fixation} \times F_{N\ fixation} + \delta^{15}N_{atm\ N} \times F_{atm\ N} + \delta^{15}N_{oceanic\ N} \times F_{oceanic\ N} = \delta^{15}N_{export\ N} \times TotN \quad (2)$$

The F parameters represent the fluxes of the different N sources that together comprise the total N input to the surface northern South China Sea. We follow (*19*) to estimate the vertical nitrate supply (204±40 mmol N m^{-2} yr^{-1}), assuming that new production is ~13% of the primary production (125±25 g C m^{-2} yr^{-1}) and the Redfield N/C ratio of 16/106. The uncertainty in this absolute rate is less important than the relative importance among the different N fluxes in the isotope balance model. Incubation-based measurements of N fixation rate range from 0.26 to 40 mmol N m^{-2} yr^{-1} (*20*), which is lower than estimates from box models using the stoichiometric relationship between N and P in the water column (*8*) or from comparing the $\delta^{15}N$ of sinking organic N with that of shallow subsurface nitrate (*9, 19*) (the latter giving an upper bound on the N fixation rate in that atmospheric N deposition was assumed to be insignificant). In some calculations, we vary the N fixation rate, but we assume that it is always below

15% of the total N input as inferred from the stoichiometric and isotopic balance calculations (*9, 19*).

To account for the 1.3‰ decrease in CS-δ^{15}N without an increase in atmospheric N deposition, the vertical nitrate flux must at least halve, or the N fixation rate must increase by at least 5 times. None of these are likely to have occurred without causing dramatic changes in the biogeochemistry in the northern South China Sea. Since it has been observed that the surface chlorophyll concentration remains relatively unchanged over the past two decades (*18*), we consider the case that both the N fixation rate increases and the vertical nitrate flux decreases to maintain a relatively constant total N flux in the mixed layer, and we assume in this case that atmospheric N deposition does not change. In this case, the 1.3‰ decrease in CS-δ^{15}N would still require at least a tripling in N fixation rate. In contrast, increasing anthropogenic N deposition is expected to relax N limitation, suppressing N fixation (*21*). A CS-δ^{15}N decline of the same magnitude has not been observed in any other open ocean environment impacted by global warming, e.g., the Sargasso Sea (*14*), indicating that changes in physical conditions are unlikely to explain the observed CS-δ^{15}N decline at Dongsha. The exercise demonstrates that our data cannot be explained by plausible changes in vertical nitrate flux and N fixation rate alone or together, pointing to the need to change atmospheric N deposition.

Atmospheric models suggest that AAN deposition to the northern South China Sea has increased approximately 4 times from 1980 to 2000 (*43*), on pace with the increase in regional AAN emissions (*6*). Regional AAN emission data do not exist prior to 1980, so the models for regional AAN deposition have greater uncertainties before 1980. Considering that agriculture and energy consumption are the main sources for AAN emissions, we can reasonably assume that the contribution from atmospheric N deposition in our studied area is negligible in the end 1960's before the δ^{15}N decline (Figure S8). We can then calculate from the 1.3‰ decline in CS-δ^{15}N that atmospheric N deposition has grown to account for 17±1% of the total N input to the surface of northern South China Sea (Case A, Figures S5A, S6A, S7A) if we hold both the vertical nitrate supply rate and N fixation rate constant. The estimate varies slightly as a function of the N fixation rate. We can undertake a similar exercise in which we allow for a decrease in vertical mixing associated with water column stratification under recent climate warming, keeping the total N fluxes from all three sources constant in order to maintain stable surface ocean production. This yields only a slightly lower estimate for the increase in atmospheric N deposition (to 15.8% of the total N) (Case B, Figure S5B, S6B, S7B), which speaks to the relatively high sensitivity of the surface ocean δ^{15}N to changes in atmospheric N input. There is very little difference in the change in the fraction of each N flux relative to the total N input in both calculations, although the two scenarios clearly differ in terms of their biological implications (Figure S5). We also consider the negative feedback in which the N fixation rate decreases with time, according to the logic that the N deposition alleviates N limitation of phytoplankton and causes a shift away from diazotrophic organisms. We do not know the sensitivity of the feedback, so we adopt a linear reduction of in-situ N fixation rate, consistent with the sensitivity test conducted in a recent model study (*21*). Under this scenario, the 1.3‰ decline in CS-δ^{15}N indicates that atmospheric N deposition has grown to account for 23±2% of the total N input to the surface of northern South China Sea (Cases C and D in Figures S5, S6, S7). Again, the

estimate varies slightly as a function of the initial N fixation rate but is insensitive to changes in vertical nitrate supply (Case C vs. D).

In summary, our N isotope model suggests that atmospheric N deposition has grown to become a significant source of fixed N to the euphotic zone in the northern South China Sea. The estimate of the fractional increase in atmospheric N deposition constrained from the isotope model is insensitive to the absolute rates assumed for the different fluxes or changes in vertical nitrate supply. The greatest dependence of the estimate is on changes in N fixation rate over time. The atmospheric N deposition is estimated to account for 17% to 23% of the total N flux, depending on whether a weak or strong negative response of N fixation to atmospheric N deposition is considered.

Decadal variation

We note that the pattern and timing of CS-$\delta^{15}N$ variation are roughly similar to decadal variations in ENSO-like conditions, with high $\delta^{15}N$ values during the warm phases (El Nino-like conditions) and low $\delta^{15}N$ values during negative phases (La Nina-like conditions) (Figure S9). Under La Nina-like conditions, strong trade winds depress the thermocline in the western Pacific and tend to enhance upper ocean density stratification in the western Pacific and South China Sea ((*44*) and the references within). This may reduce vertical mixing and its capacity to import nutrients to the euphotic zone, thus increasing the relative importance of ^{15}N-depleted N sources from N fixation and atmospheric N deposition. However, there are probably plausible alternatives. Hydrographic observations on the relationship between water column stratification and N dynamics may be needed to evaluate the role of such teleconnections.

Potential changes in reef ecology

Dongsha Atoll experienced a bleaching event in 1998 (*45*), but the lack of a clear signal in the skeletal growth rate suggests that it was not well-captured in our sampling of the coral core, nor did that event strongly affect the growth of this coral in subsequent years (Figure S10). This argues against a N isotopic impact from changing coral host/symbiont N fluxes, which if it occurred would have been expected to raise the $\delta^{15}N$ of the coral host by reducing internal nitrogen recycling (*13*), the opposite of the observed trend. While bleaching could have caused permanent changes in reef biogeochemistry, the rapid exchange between its interior lagoon and the open ocean and the uniformly low dissolved inorganic N in surface waters argue against a significant effect of the reef cover on the $\delta^{15}N$ of the forms of N available to corals, as supported by the similarity in CS-$\delta^{15}N$ between the coral cores from the two distinct sites on the atoll (Figure S1), and the similar nitrate $\delta^{15}N$ values observed both within and outside the lagoon.

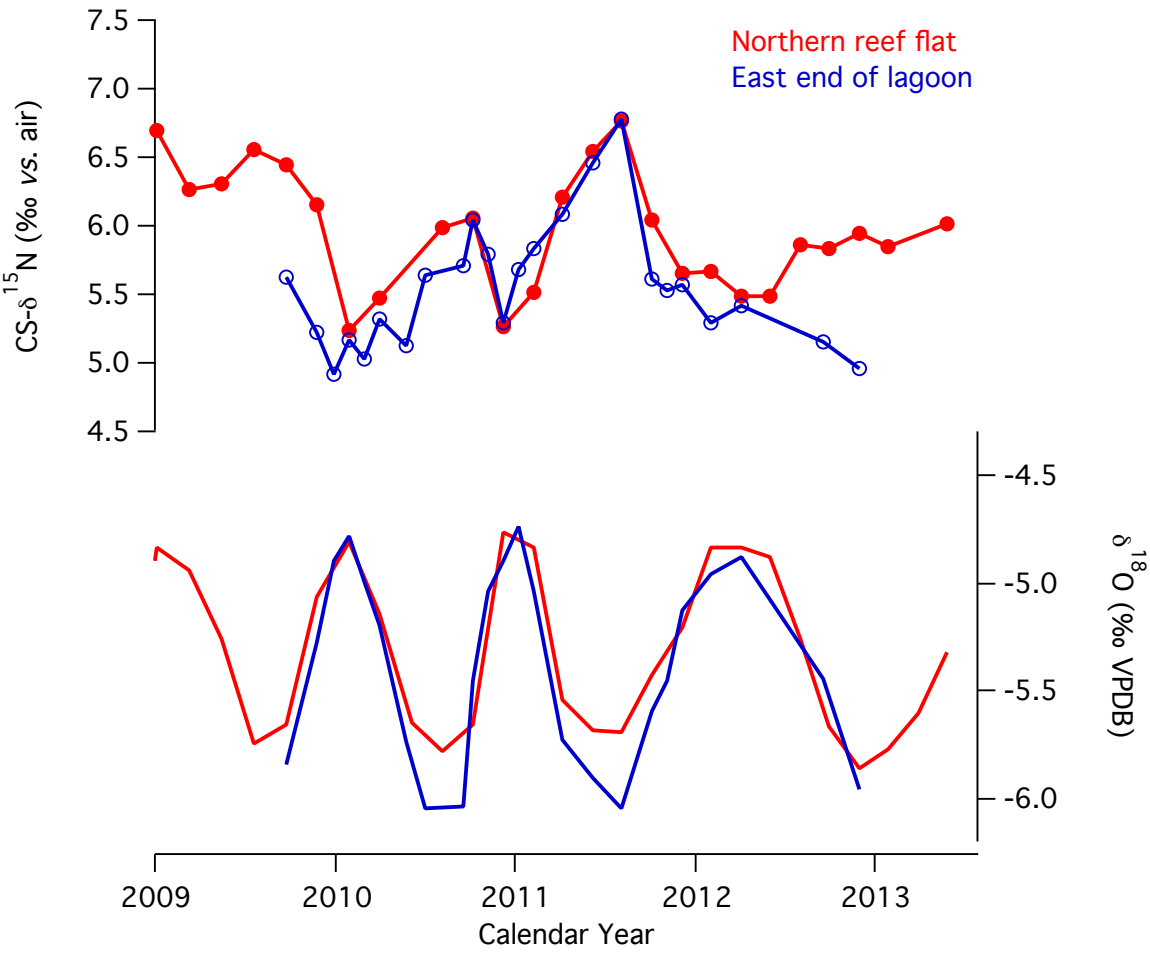

Figure S1. CS-δ^{15}N and skeletal aragonite δ^{18}O generated from two *Porites* cores at the north reef flat (red) and east end of the lagoon (blue).

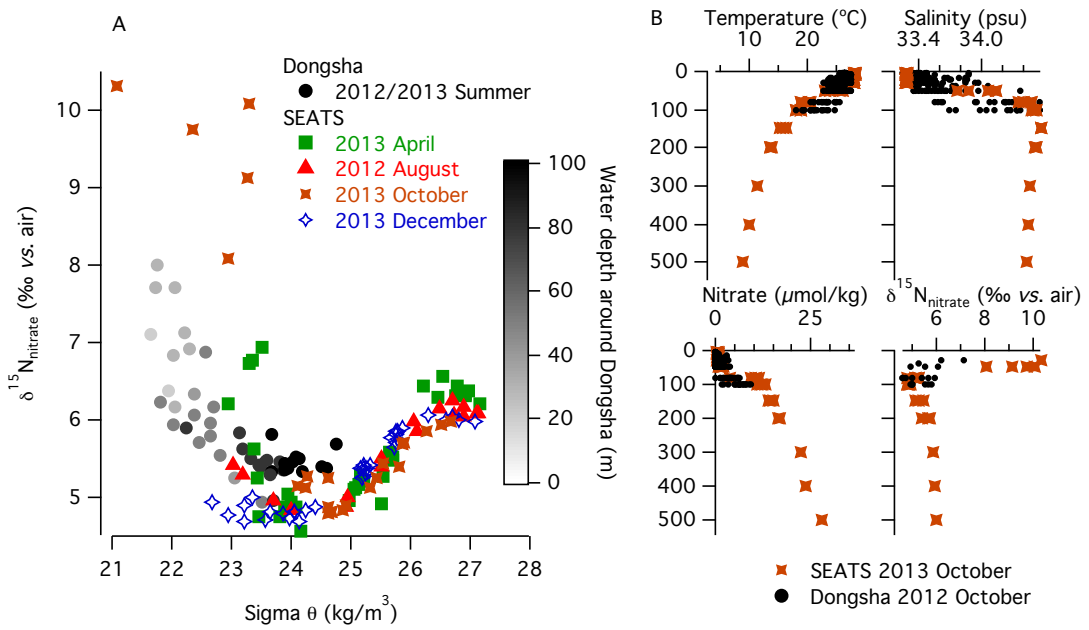

Figure S2. Hydrography of Dongsha Atoll and the northern South China Sea. A) Nitrate $\delta^{15}N$ versus water density near Dongsha and within the Dongsha lagoon (black) and at SEATS (18°N, 116°E) during four occupations. The slightly (<0.5‰) higher nitrate $\delta^{15}N$ at Dongsha relative to SEATS for the shallow thermocline (sigma-theta near 24) is probably due to internal wave-aided vertical mixing over the margin, weakening the nitrate $\delta^{15}N$ minimum of the shallow thermocline near Dongsha and leading to more scatter. B) Depth profiles of temperature, salinity, nitrate, and nitrate $\delta^{15}N$ near Dongsha (black circles: stations are shown in Figure 1B) and at SEATS (orange crosses). Vertical mixing is stronger near the atoll, explaining the greater scatter in the Dongsha profiles.

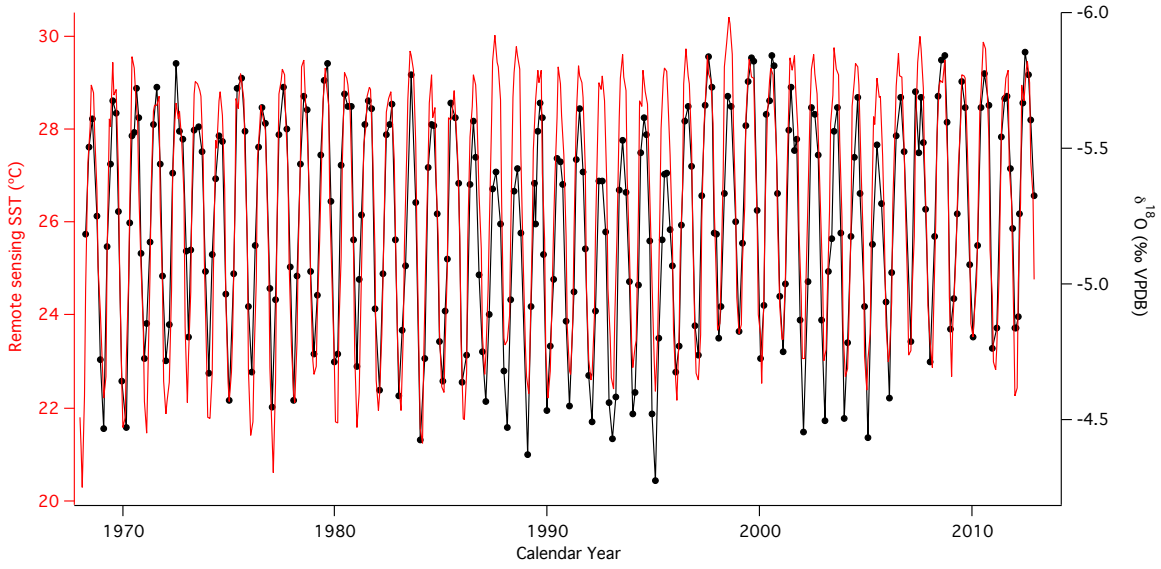

Figure S3. Basis for the age model for the Dongsha coral core. The age model was determined by counting annual growth bands in CAT scan images and by correlating $\delta^{18}O$ with satellite sea-surface temperature (http://www.metoffice.gov.uk/hadobs/hadisst/) by matching midpoints of $\delta^{18}O$ and SST.

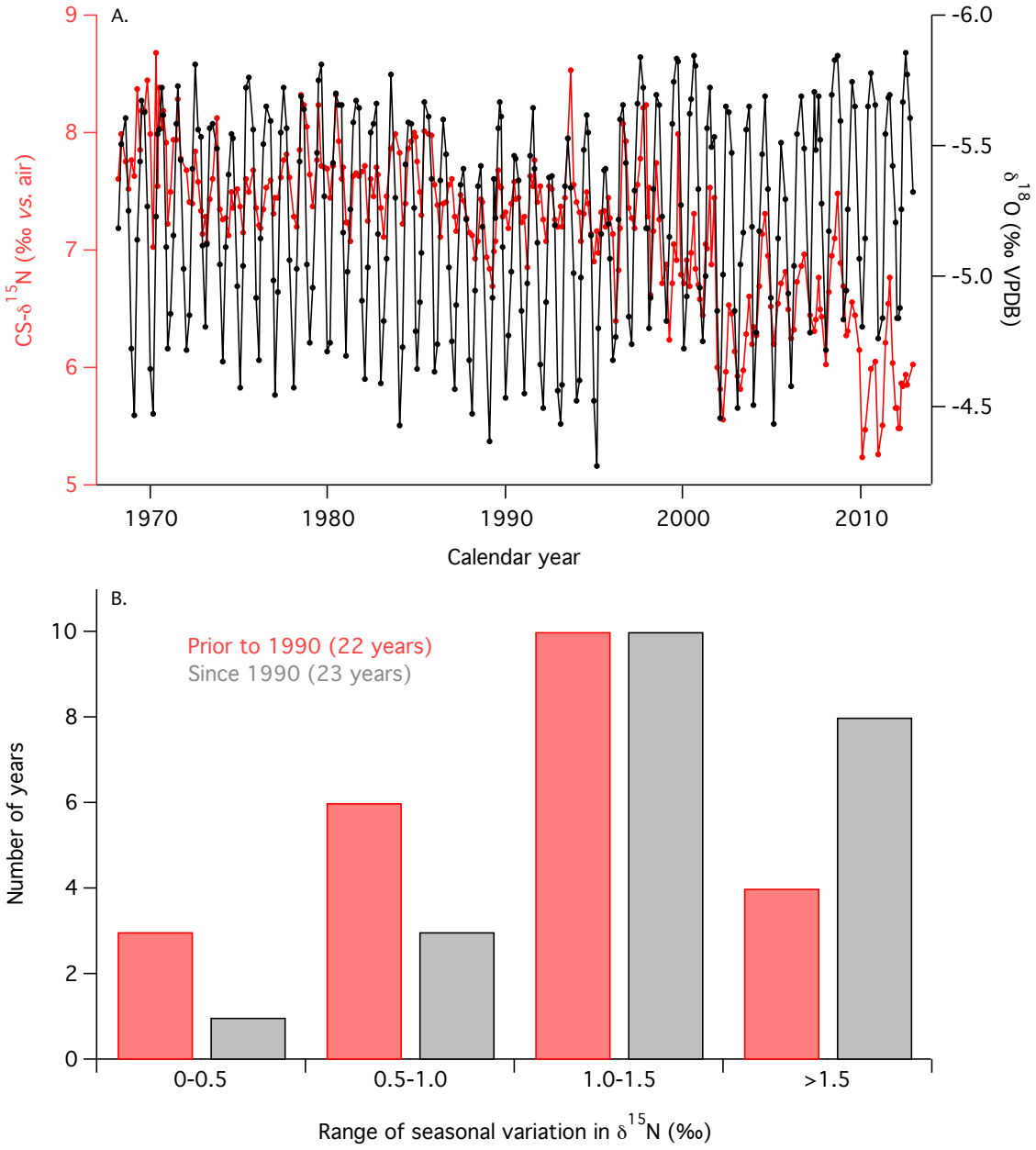

Figure S4. The strong correlation between seasonal variation in CS-δ^{15}N and aragonite δ^{18}O, and the increase in seasonal δ^{15}N variation since 1990. (A) High CS-δ^{15}N is associated with and slightly lags δ^{18}O minima, such that δ^{15}N maxima occur in the late summer/autumn and δ^{15}N minima occur in late winter/spring. (B) Histogram showing number of years with a given range in seasonal variation in δ^{15}N (difference between maximum and minimum) prior to and since 1990.

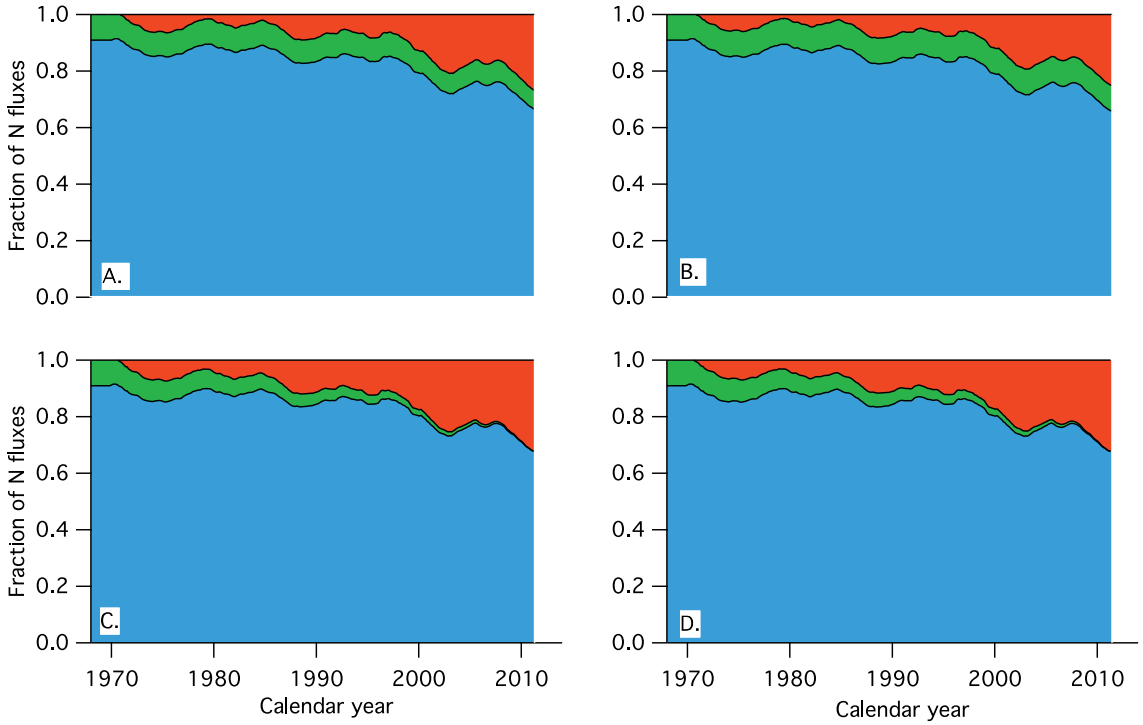

Figure S5. Fractional changes in the major N fluxes in the South China Sea constrained from CS-δ^{15}N change, using a euphotic zone N isotope balance model. Atmospheric N deposition, N fixation, and vertical nitrate supply, are shown in red, green, and blue. Case (A): Only atmospheric N deposition is allowed to change. This case is shown in Figure 3 upper panel. Case (B): N fixation rate and the total N input to the euphotic zone (including atmospheric N deposition) are held constant. The reduction in vertical nitrate supply resulting from upper ocean stratification is perfectly compensated by an increase in atmospheric N deposition. Case (C): Vertical nitrate flux is held constant. N fixation rate decreases linearly to zero over this period, presumably in response to increasing atmospheric N deposition. Case (D): The total N input to the euphotic zone is held constant. The reduction in vertical nitrate supply and linear decrease in N fixation rate are compensated by the increase in atmospheric N deposition.

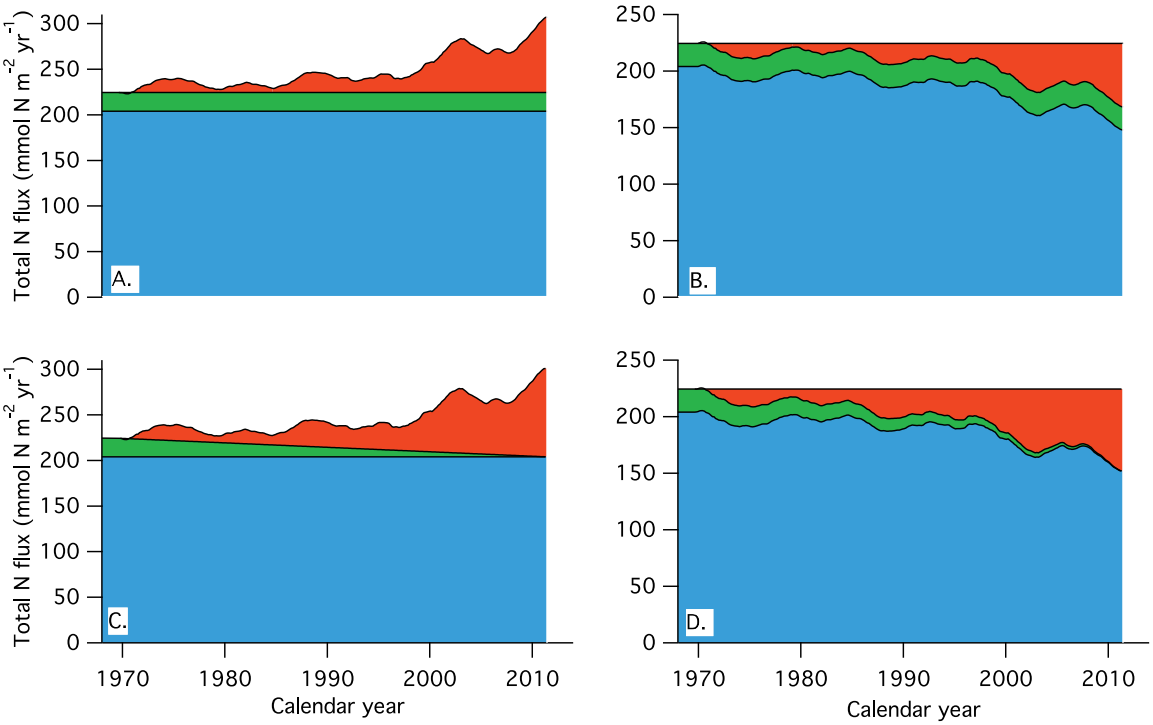

Figure S6. Absolute changes in the major N fluxes in the South China Sea constrained from CS-δ^{15}N change, using a euphotic zone N isotope balance model. Atmospheric N deposition, N fixation, and vertical nitrate supply, are shown in red, green, and blue. The calculations are the same as in Figure S5, but with absolute rates shown. Case A is shown in Figure 3. Vertical nitrate flux is assumed to be 204 mmol N m^{-2} yr^{-1} (*19*). N fixation rate at the beginning of the period is assumed to be 20 mmol N m^{-2} yr^{-1}, the median from incubation measurements and box model calculations (*19, 20*).

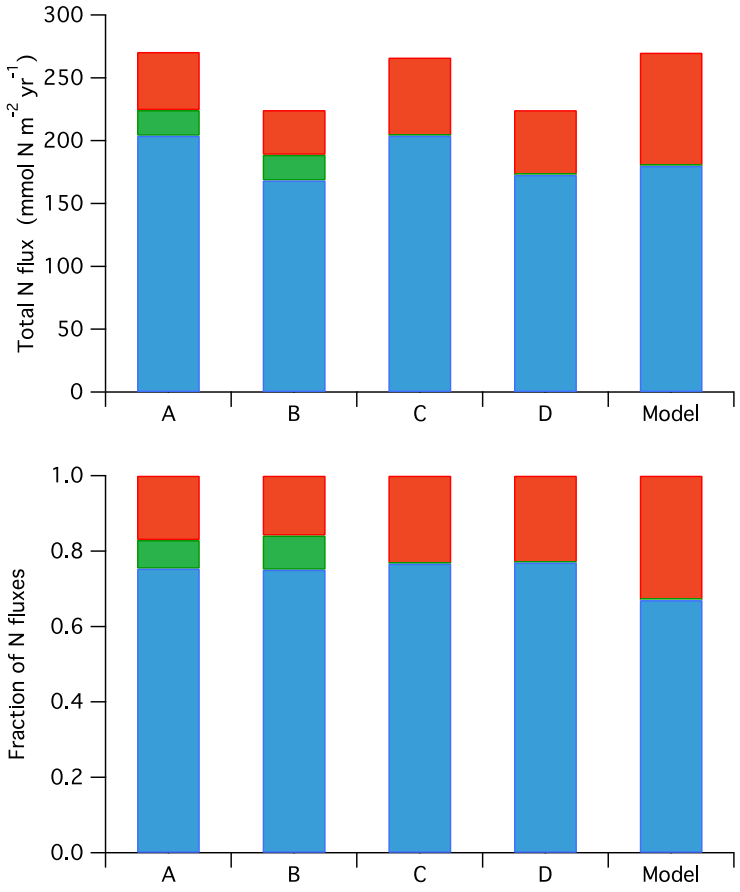

Figure S7. The N fluxes (upper panel) and their relative fractions (lower panel) computed using a euphotic zone N isotope balance model, compared with the estimate from an atmospheric model for the year 2000 (*1*). Atmospheric N deposition, N fixation, and vertical nitrate supply, are shown in red, green, and blue. Case A-D are as calculated for as in Figure S5 and S6, using the 1.3‰ decrease recorded in CS-δ^{15}N.

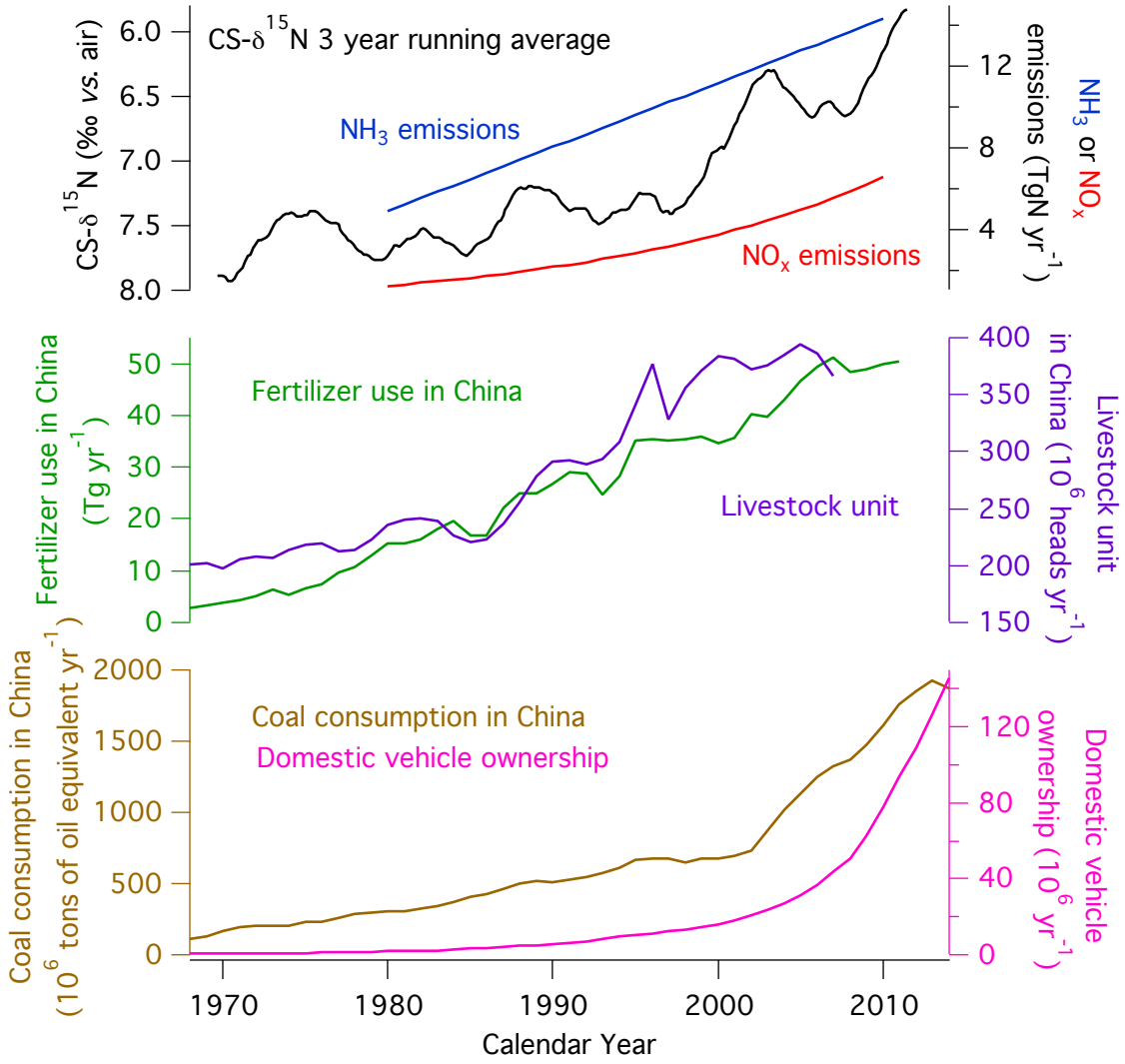

Figure S8. Comparison of the long term CS-δ^{15}N decline with anthropogenic N emissions (*5*) and their major contributors in China. The δ^{15}N decline (black curve) follows the increase in NO_x emissions (red curve), which is primarily driven by the growth in coal consumption and vehicle usage in China (lower panel). Note that the smoothed CS-δ^{15}N record is plotted decreasing upward. Data on fertilizer use (green), livestock (purple), and coal consumption (brown) are compiled by Earth Policy Institute (downloaded from http://www.earth-policy.org/data_center/), and the number of vehicles is from the National Bureau of Statistics of China (http://www.stats.gov.cn/english/).

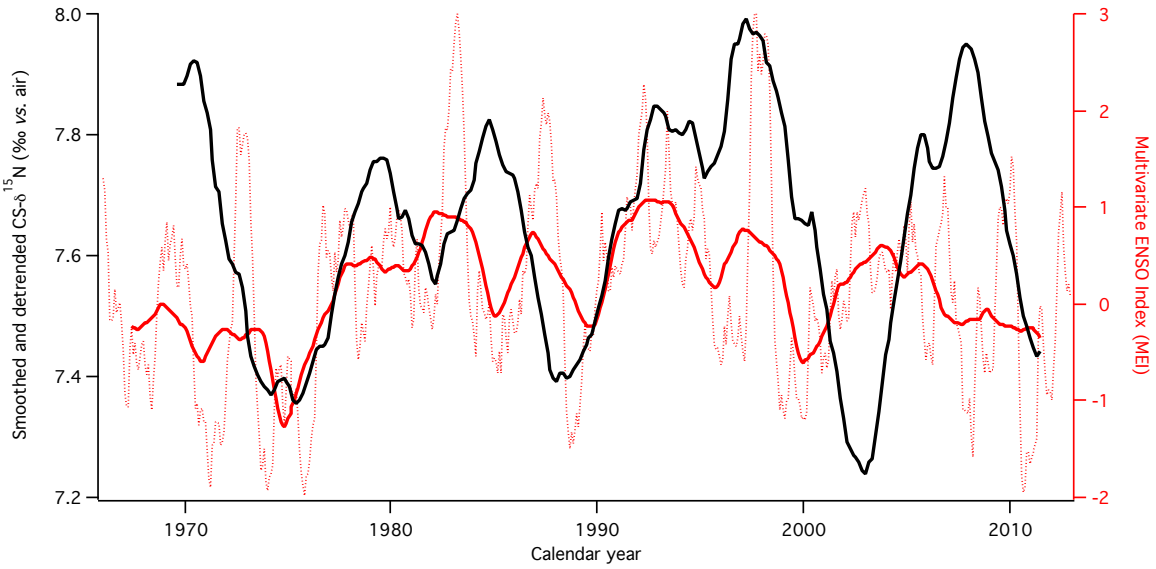

Figure S9. Decadal CS-δ^{15}N variation may be related to decadal changes in ENSO. The smoothed and detrended CS-δ^{15}N (black) shows positive correlation with changes in ENSO activity, with high δ^{15}N values during El Nino-like conditions and low values in La Nino-like conditions. Smoothed MEI (solid red curve) is calculated from the 3 year running average of the MEI time series (dashed red line) (downloaded from http://www.esrl.noaa.gov/psd/enso/mei/).

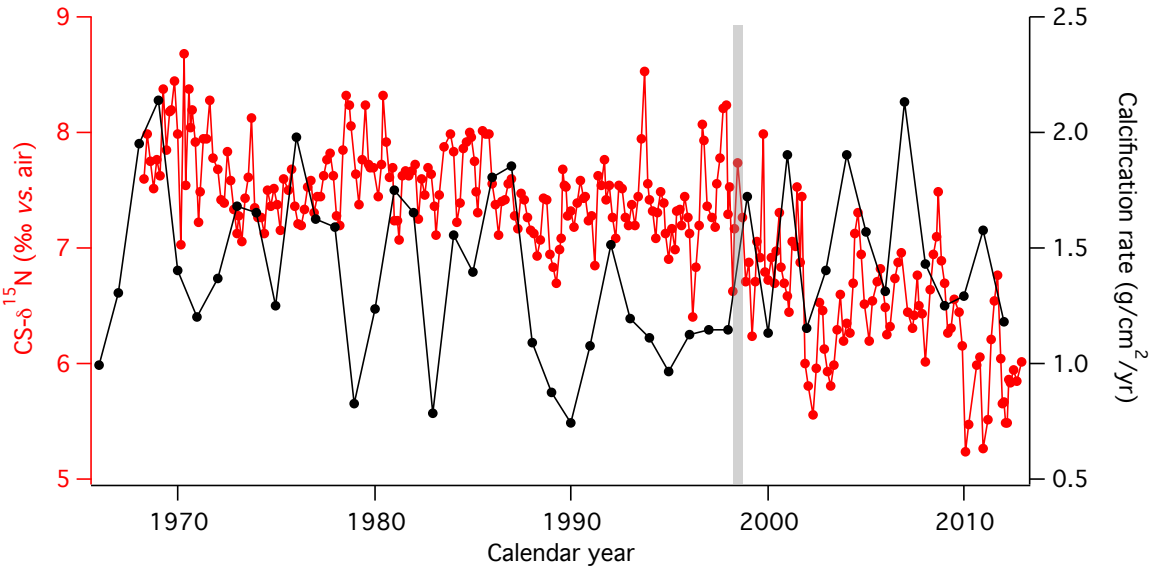

Figure S10. No correlation is observed between CS-δ^{15}N and calcification rate. Among other implications, the data suggest that the 1998 coral bleaching event (indicated by the gray bar) did not influence coral growth or CS-δ^{15}N.

References and Notes

1. R. A. Duce, J. LaRoche, K. Altieri, K. R. Arrigo, A. R. Baker, D. G. Capone, S. Cornell, F. Dentener, J. Galloway, R. S. Ganeshram, R. J. Geider, T. Jickells, M. M. Kuypers, R. Langlois, P. S. Liss, S. M. Liu, J. J. Middelburg, C. M. Moore, S. Nickovic, A. Oschlies, T. Pedersen, J. Prospero, R. Schlitzer, S. Seitzinger, L. L. Sorensen, M. Uematsu, O. Ulloa, M. Voss, B. Ward, L. Zamora, Impacts of atmospheric anthropogenic nitrogen on the open ocean. *Science* **320**, 893–897 (2008). doi:10.1126/science.1150369 Medline

2. A. Krishnamurthy, J. K. Moore, N. Mahowald, C. Luo, C. S. Zender, Impacts of atmospheric nutrient inputs on marine biogeochemistry. *J. Geophys. Res. Biogeosci.* **115**, G01006 (2010).

3. H. W. Paerl, Coastal eutrophication and harmful algal blooms: Importance of atmospheric deposition and groundwater as "new" nitrogen and other nutrient sources. *Limnol. Oceanogr.* **42**, 1154–1165 (1997). doi:10.4319/lo.1997.42.5_part_2.1154

4. A. Richter, J. P. Burrows, H. Nüss, C. Granier, U. Niemeier, Increase in tropospheric nitrogen dioxide over China observed from space. *Nature* **437**, 129–132 (2005). doi:10.1038/nature04092 Medline

5. X. Liu, Y. Zhang, W. Han, A. Tang, J. Shen, Z. Cui, P. Vitousek, J. W. Erisman, K. Goulding, P. Christie, A. Fangmeier, F. Zhang, Enhanced nitrogen deposition over China. *Nature* **494**, 459–462 (2013). doi:10.1038/nature11917 Medline

6. X. Liu, L. Duan, J. Mo, E. Du, J. Shen, X. Lu, Y. Zhang, X. Zhou, C. He, F. Zhang, Nitrogen deposition and its ecological impact in China: An overview. *Environ. Pollut.* **159**, 2251–2264 (2011). doi:10.1016/j.envpol.2010.08.002 Medline

7. T. W. Kim, K. Lee, R. Duce, P. Liss, Impact of atmospheric nitrogen deposition on phytoplankton productivity in the South China Sea. *Geophys. Res. Lett.* **41**, 3156–3162 (2014). doi:10.1002/2014GL059665

8. I. N. Kim, K. Lee, N. Gruber, D. M. Karl, J. L. Bullister, S. Yang, T.-W. Kim, Chemical oceanography. Increasing anthropogenic nitrogen in the North Pacific Ocean. *Science* **346**, 1102–1106 (2014). doi:10.1126/science.1258396 Medline

9. G. T. F. Wong, S.-W. Chung, F.-K. Shiah, C.-C. Chen, L.-S. Wen, K.-K. Liu, Nitrate anomaly in the upper nutricline in the northern South China Sea - Evidence for nitrogen fixation. *Geophys. Res. Lett.* **29**, 12-1–12-4 (2002). doi:10.1029/2002GL015796

10. E. Wada, M. Terazaki, Y. Kabaya, T. Nemoto, ^{15}N and ^{13}C abundances in the Antartic Ocean with emphasis on the biogeochemical structure of the food web. *Deep-Sea Res. A, Oceanogr. Res. Pap.* **34**, 829–841 (1987). doi:10.1016/0198-0149(87)90039-2

11. J. Y. T. Yang, S. C. Hsu, M. H. Dai, S. S. Y. Hsiao, S. J. Kao, Isotopic composition of water-soluble nitrate in bulk atmospheric deposition at Dongsha Island:

Sources and implications of external N supply to the northern South China Sea. *Biogeosciences* **11**, 1833–1846 (2014). doi:10.5194/bg-11-1833-2014

12. A. Yamazaki, T. Watanabe, U. Tsunogai, Nitrogen isotopes of organic nitrogen in reef coral skeletons as a proxy of tropical nutrient dynamics. *Geophys. Res. Lett.* **38**, L19605 (2011). doi:10.1029/2011GL049053

13. X. T. Wang, D. M. Sigman, A. L. Cohen, D. J. Sinclair, R. M. Sherrell, M. A. Weigand, D. V. Erler, H. Ren, Isotopic composition of skeleton-bound organic nitrogen in reef-building symbiotic corals: A new method and proxy evaluation at Bermuda. *Geochim. Cosmochim. Acta* **148**, 179–190 (2015). doi:10.1016/j.gca.2014.09.017

14. X. T. Wang, D. M. Sigman, A. L. Cohen, D. J. Sinclair, R. M. Sherrell, K. M. Cobb, D. V. Erler, J. Stolarski, M. V. Kitahara, H. Ren, Influence of open ocean nitrogen supply on the skeletal δ 15 N of modern shallow-water scleractinian corals. *Earth Planet. Sci. Lett.* **441**, 125–132 (2016). doi:10.1016/j.epsl.2016.02.032

15. Materials and methods are available as supplementary materials.

16. T. M. DeCarlo, K. B. Karnauskas, K. A. Davis, G. T. F. Wong, Climate modulates internal wave activity in the Northern South China Sea. *Geophys. Res. Lett.* **42**, 831–838 (2015). doi:10.1002/2014GL062522

17. W. W. Gregg, M. E. Conkright, Decadal changes in global ocean chlorophyll. *Geophys. Res. Lett.* **29**, 20-1–20-4 (2002). doi:10.1029/2002GL014689

18. K. K. Liu, L.-W. Wang, M. Dai, C.-M. Tseng, Y. Yang, C.-H. Sui, L. Oey, K.-Y. Tseng, S.-M. Huang, Inter-annual variation of chlorophyll in the northern South China Sea observed at the SEATS Station and its asymmetric responses to climate oscillation. *Biogeosciences* **10**, 7449–7462 (2013). doi:10.5194/bg-10-7449-2013

19. G. T. F. Wong, C. M. Tseng, L. S. Wen, S. W. Chung, Nutrient dynamics and N-anomaly at the SEATS station. *Deep Sea Res. Part II Top. Stud. Oceanogr.* **54**, 1528–1545 (2007). doi:10.1016/j.dsr2.2007.05.011

20. Y.-L. L. Chen, Spatial and seasonal variations of nitrate-based new production and primary production in the South China Sea. *Deep Sea Res. Part I Oceanogr. Res. Pap.* **52**, 319–340 (2005). doi:10.1016/j.dsr.2004.11.001

21. S. Yang, N. Gruber, The anthropogenic perturbation of the marine nitrogen cycle by atmospheric deposition: Nitrogen cycle feedbacks and the ^{15}N Haber-Bosch effect. *Global Biogeochem. Cycles* **30**, 1418–1440 (2016). doi:10.1002/2016GB005421

22. G. W. Holtgrieve, D. E. Schindler, W. O. Hobbs, P. R. Leavitt, E. J. Ward, L. Bunting, G. Chen, B. P. Finney, I. Gregory-Eaves, S. Holmgren, M. J. Lisac, P. J. Lisi, K. Nydick, L. A. Rogers, J. E. Saros, D. T. Selbie, M. D. Shapley, P. B. Walsh, A. P. Wolfe, A coherent signature of anthropogenic nitrogen deposition to remote watersheds of the Northern Hemisphere. *Science* **334**, 1545–1548 (2011). doi:10.1126/science.1212267 Medline

23. M. G. Hastings, J. C. Jarvis, E. J. Steig, Anthropogenic impacts on nitrogen isotopes of ice-core nitrate. *Science* **324**, 1288 (2009). doi:10.1126/science.1170510 Medline

24. Y. Fang, M. Yoh, K. Koba, W. Zhu, Y. Takebayashi, Y. Xiao, C. Lei, J. Mo, W. Zhang, X. Lu, Nitrogen deposition and forest nitrogen cycling along an urban-rural transect in southern China. *Glob. Change Biol.* **17**, 872–885 (2011). doi:10.1111/j.1365-2486.2010.02283.x

25. F. Dentener, J. Drevet, J. F. Lamarque, I. Bey, B. Eickhout, A. M. Fiore, D. Hauglustaine, L. W. Horowitz, M. Krol, U. C. Kulshrestha, M. Lawrence, C. Galy-Lacaux, S. Rast, D. Shindell, D. Stevenson, T. Van Noije, C. Atherton, N. Bell, D. Bergman, T. Butler, J. Cofala, B. Collins, R. Doherty, K. Ellingsen, J. Galloway, M. Gauss, V. Montanaro, J. F. Müller, G. Pitari, J. Rodriguez, M. Sanderson, F. Solmon, S. Strahan, M. Schultz, K. Sudo, S. Szopa, O. Wild, Nitrogen and sulfur deposition on regional and global scales: A multimodel evaluation. *Global Biogeochem. Cycles* **20**, GB4003 (2006). doi:10.1029/2005GB002672

26. T. D. Jickells, E. Buitenhuis, K. Altieri, A. R. Baker, D. Capone, R. A. Duce, F. Dentener, K. Fennel, M. Kanakidou, J. LaRoche, K. Lee, P. Liss, J. J. Middelburg, J. K. Moore, J. Okin, A. Oschlies, M. Sarin, S. Seitzinger, J. Sharples, A. Singh, P. Suntharalingam, Uematsu, L. M. Zamora, A reevaluation of the magnitude and impacts of anthropogenic atmospheric nitrogen inputs on the ocean. *Global Biogeochem. Cycles* **31**, 289–303 (2017).

27. M. G. Hastings, D. M. Sigman, F. Lipschultz, Isotopic evidence for source changes of nitrate in rain at Bermuda. *J. Geophys. Res. Atmos.* **108** (D24), 4790 (2003). doi:10.1029/2003JD003789

28. K. E. Altieri, S. E. Fawcett, A. J. Peters, D. M. Sigman, M. G. Hastings, Marine biogenic source of atmospheric organic nitrogen in the subtropical North Atlantic. *Proc. Natl. Acad. Sci. U.S.A.* **113**, 925–930 (2016). doi:10.1073/pnas.1516847113 Medline

29. Y. Jia, G. Yu, Y. Gao, N. He, Q. Wang, C. Jiao, Y. Zuo, Global inorganic nitrogen dry deposition inferred from ground- and space-based measurements. *Sci. Rep.* **6**, 19810 (2016). doi:10.1038/srep19810 Medline

30. I.-I. Lin, J.-P. Chen, G. T. F. Wong, C.-W. Huang, C.-C. Lien, Aerosol input to the South China Sea: Results from the MODerate Resolution Imaging Spectro-radiometer, the Quick Scatterometer, and the measurements of pollution in the troposphere sensor. *Deep Sea Res. Part II Top. Stud. Oceanogr.* **54**, 1589 (2007). doi:10.1016/j.dsr2.2007.05.013

31. J. J. Elser, T. Andersen, J. S. Baron, A.-K. Bergström, M. Jansson, M. Kyle, K. R. Nydick, L. Steger, D. O. Hessen, Shifts in lake N:P stoichiometry and nutrient limitation driven by atmospheric nitrogen deposition. *Science* **326**, 835–837 (2009). doi:10.1126/science.1176199 Medline

32. H. W. Paerl, R. L. Dennis, D. R. Whitall, Atmospheric deposition of nitrogen: Implications for nutrient over-enrichment of coastal waters. *Estuaries* **25**, 677–693 (2002). doi:10.1007/BF02804899

33. B. Mouriño-Carballido, M. Pahlow, A. Oschlies, High sensitivity of ultra-oligotrophic marine ecosystems to atmospheric nitrogen deposition. *Geophys. Res. Lett.* **39**, L05601 (2012).

34. T. M. DeCarlo, A. L. Cohen, H. C. Barkley, Q. Cobban, C. Young, K. E. Shamberger, R. E. Brainard, Y. Golbuu, Coral macrobioerosion is accelerated by ocean acidification and nutrients. *Geology* **43**, 7–10 (2014). doi:10.1130/G36147.1

35. T. M. DeCarlo, A. L. Cohen, coralCT: Software tool to analyze computerized tomography (CT) scans of coral skeletal cores for calcification and bioerosion rates. Zenodo (2016); https://zenodo.org/record/57855.

36. R. S. Braman, S. A. Hendrix, Nanogram nitrite and nitrate determination in environmental and biological materials by vanadium (III) reduction with chemiluminescence detection. *Anal. Chem.* **61**, 2715–2718 (1989). doi:10.1021/ac00199a007 Medline

37. D. M. Sigman, K. L. Casciotti, M. Andreani, C. Barford, M. Galanter, J. K. Böhlke, A bacterial method for the nitrogen isotopic analysis of nitrate in seawater and freshwater. *Anal. Chem.* **73**, 4145–4153 (2001). doi:10.1021/ac010088e Medline

38. K. L. Casciotti, D. M. Sigman, M. G. Hastings, J. K. Böhlke, A. Hilkert, Measurement of the oxygen isotopic composition of nitrate in seawater and freshwater using the denitrifier method. *Anal. Chem.* **74**, 4905–4912 (2002). doi:10.1021/ac020113w Medline

39. S. E. Fawcett, M. W. Lomas, B. B. Ward, D. M. Sigman, The counterintuitive effect of summer-to-fall mixed layer deepening on eukaryotic new production in the Sargasso Sea. *Global Biogeochem. Cycles* **28**, 86–102 (2014). doi:10.1002/2013GB004579

40. A. R. Gobel, K. E. Altieri, A. J. Peters, M. G. Hastings, D. M. Sigman, Insights into anthropogenic nitrogen deposition to the North Atlantic investigated using the isotopic composition of aerosol and rainwater nitrate. *Geophys. Res. Lett.* **40**, 5977–5982 (2013). doi:10.1002/2013GL058167

41. J. H. Carrillo, M. G. Hastings, D. M. Sigman, B. J. Huebert, Atmospheric deposition of inorganic and organic nitrogen and base cations in Hawaii. *Global Biogeochem. Cycles* **16**, 24-1–24-16 (2002). doi:10.1029/2002GB001892

42. K. E. Altieri, M. G. Hastings, A. R. Gobel, A. J. Peters, D. M. Sigman, Isotopic composition of rainwater nitrate at Bermuda: The influence of air mass source and chemistry in the marine boundary layer. *J. Geophys. Res. Atmos.* **118**, 11304–11316 (2013). doi:10.1002/jgrd.50829

43. J. F. Lamarque, F. Dentener, J. McConnell, C.-U. Ro, M. Shaw, R. Vet, D. Bergmann, P. Cameron-Smith, R. Doherty, G. Faluvegi, S. J. Ghan, B. Josse, Y. H. Lee, I. A. MacKenzie, D. Plummer, D. T. Shindell, D. S. Stevenson, S. Strode,

G. Zeng, Multi-model mean nitrogen and sulfur deposition from the Atmospheric Chemistry and Climate Model Intercomparison Project (ACCMIP): Evaluation historical and projected changes. *Atmos. Chem. Phys.* **13**, 6247–6294 (2013). doi:10.5194/acpd-13-6247-2013

44. I.-I. Lin, J.-C. Chan, Recent decrease in typhoon destructive potential and global warming implications. *Nat. Commun.* **6**, 7182 (2015). doi:10.1038/ncomms8182 Medline

45. J.-J. Li, T.-F. Lee, K. S. Tew, L.-S. Fang, Changes in the coral community at Dong-Sha Atoll, South China Sea from 1975 to 1998. *Acta Zool. Taiwanica* **11**, 1–15 (2000).